Characteristics of Satellite-derived Clear-sky Atmospheric Temperature Inversion Strength in the Arctic, 1980-1996

Yinghui Liu[1], Jeffrey R. Key[2] , Axel Schweiger[3], Jennifer Francis[4]

[1]Cooperative Institute for Meteorological Satellite Studies, University of Wisconsin-Madison
1225 West Dayton Street, Madison, WI, 53706, USA
[2]Office of Research and Applications, NOAA/NESDIS
1225 West Dayton Street, Madison, WI, 53706, USA
[3]Polar Science Center, University of Washington, Seattle, Washington, USA
[4]Rutgers University, NewBrunswick, New Jersey, USA

Abstract

The low-level atmospheric temperature inversions are the dominant feature of the atmosphere field in Arctic throughout most of the year. The spatial distribution, temporal characteristics, and changes over time of the temperature inversion are important to many of the researches related to the Polar Regions. However, sparse data from meteorological satations poleward of 70°N, especially over ocean, can not provide such information, Satellite-borne sensors provide an appealing opportunity to study the temperature inversions in the polar region. This study focuses on the spatial and temporal characteristics, and change from 1980 through 1996, of satellite-derived clear-sky atmospheric temperature inversion strength in Arctic in the cold season. The 17-year time series of clear-sky temperature inversion strength in the cold season in Arctic is derived from TIROS-N operational vertical sounder (TOVS) data using 2-channel statistical method. The spatial distributions of the monthly mean satellite-derived clear-sky inversion strength in Arctic in November, December, January, February, March, and in the winter season are presented. The inversion strength trends based on the monthly mean data are also derived and shown. Both increasing and decreasing trends are revealed in the cold season for different regions in Arctic.

Introduction

Low-level atmospheric temperature inversions are ubiquitous at high latitudes during the polar winter, and are the dominant feature of the atmospheric temperature field in the Arctic (Curry et al. 1996). Temperature inversions in the polar regions may result from radiative cooling, warm air advection over a cooler surface layer, subsidence, cloud process, surface melt and topography (Vowinkel and Orvig 1970; Maykut and Church 1973; Busch et al. 1982; Curry 1983; Kahl 1990; Serreze et al. 1992). Temperature inversions influence the magnitude of heat and moisture fluxes through openings in the sea ice, the depth of vertical mixing in the boundary layer, pollution gases and aerosol transport, photochemical destruction of boundary-layer ozone at Arctic sunrise, surface wind velocity, and lead formation (Andreas 1980; Andreas and Murphy 1986; Barrie et al. 1988; Barry and Miles, 1988).

Temperature inversion information can be directly derived from radiosonde data, but such radiosonde data are rare over ocean and sparse over land in Arctic. Satellites provide an appealing opportunity to monitor the clear-sky temperature inversions in the polar regions. Liu and Key (2003, hereinafter referred to as LK03) developed an empirical algorithm to detect and estimate the characteristics of clear-sky, low-level temperature inversions using the data from the Moderate Resolution Imaging Spectroradiometer (MODIS) on the Terra and Aqua satellites. However, MODIS does not provide a long enough time series for climatological analyses. The TIROS-N Operational Vertical Sounder (TOVS), which provides continuous measurements of the earth's surface and atmosphere since 1979, has the similar channels used by the MODIS algorithm, which provides an opportunity to study the long-term change of temperature inversion.

In this paper we adapt the empirical method developed for MODIS to TOVS data for the period 1980-1996, thereby providing the opportunity to study the spatial distribution and temporal trends of clear-sky, low-level temperature inversion characteristics. Of primary interest is the inversion strength (INVST), defined as the temperature difference between the surface and top the inversion.

Data

The radiosonde data in this study are obtained from Historical Arctic Rawinsonde Archive (HARA). All the soundings are processed with quality control using the method described by Serreze et al (1992). The twice-daily soundings data from 1979 to 1996 from 61 stations are used to match the TOVS data. In this study, the inversion base is defined by the station elevation, and the inversion top is the atmosphere layer, which is lower than 700 hPa, with the maximum temperature. Isothermal layers at the base, atop, or embedded within an inversion layer are included. Thin layers with a decrease of temperature with height provided they are not more than 100m in depth are included.

TOVS brightness temperatures (BT) at 7.3 μm and 11 μm are used in the inversion strength retrieval. The TOVS data used in this study includes NOAA-6 (1979-1982), NOAA-7 (1983-1984), NOAA-9 (1985-1986), NOAA-10 (1987-1991), NOAA-11 (1992-1994) and NOAA-12 (1995-1996) data. The spatial resolution of the original TOVS brightness temperature data is 17 km at nadir. Cloud detection tests described by Chedin et al. (1985) and Francis (1994) are applied to distinguish clear from cloudy scenes.

Theoretical Basis And Method

Under clear conditions, temperature inversion strength can be estimated using brightness temperatures from satellite data. The peaks of the weighting functions for the 7.3, 11 μm channels are approximately 650 hPa, and the surface, respectively. The brightness temperature of the window channel at 11 μm, BT_{11}, will be most sensitive to the temperature of the surface. The 7.3 μm water vapor channel brightness temperature, $BT_{7.3}$, has most contribution from the layers around 650 hPa. The magnitude of the brightness temperature difference (BTD) between the 7.3 μm and 11 μm channels, $BT_{7.3}$-BT_{11}, will therefore be related to the temperature difference of the inversion top and the surface, which is related to the inversion strength.

The inversion strength retrieval algorithm described by Liu and Key (2003) is based on radiosonde-satellite data matched pairs, and similar approach is used in this study. Radiosonde data from 61 stations in Arctic, and TOVS brightness temperature data from 1980 though 1996 are used to find the matched pairs between inversion strength derived from radiosonde data and TOVS BTs under only clear-sky conditions. Figure 1 shows the relationship between inversion strength and $BT_{7.3}$-BT_{11} for the cases in all seasons of a year, and for the cases in the cold season, which only includes November, December, January, February, and March. For the matched cases of all seasons (Figure 1(a)), when $BT_{7.3}$ - BT_{11} is larger than –10 K, the inversion strength is well linearly related to $BT_{7.3}$ - BT_{11}; when $BT_{7.3}$ - BT_{11} is less than –10 K, there is no linear relationship between inversion strength and $BT_{7.3}$ - BT_{11}. For the matched cases in the cold season (Figure 1(b)), most cases have $BT_{7.3}$ - BT_{11} larger than –10 K, which leads to a good linear relationship between inversion strength and $BT_{7.3}$ - BT_{11}. The different relationships of $BT_{7.3}$ - BT_{11} and inversion strength between the cold season and warm season might come from the difference of moisture profiles in cold season and warm season where the warm season includes the months not included in the cold season. In the cold season, the water vapor content of the whole atmosphere column is low, which might enable the $BT_{7.3}$ reflect the information of the inversion top; while in the warm season, the high water vapor content of the atmosphere might weaken the ability of $BT_{7.3}$ to see the inversion top. For this reason, this study only focuses on the inversion strength in the cold season.

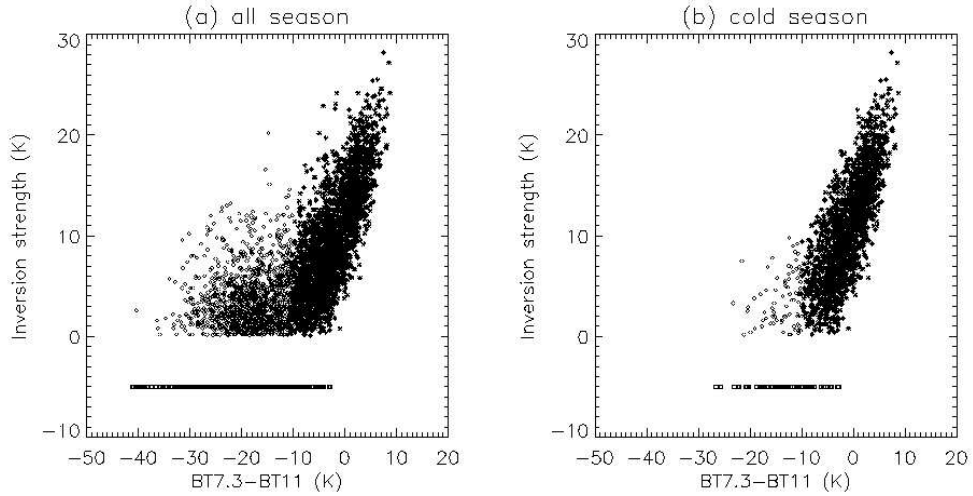

Fig. 1: Relationship between inversion strength and $BT_{7.3}$-BT_{11} for (a) all seasons, and (b) for cold season. The square represents the cases without temperature inversion. The diamond represents the case with $BT_{7.3}$-BT_{11} less than –10 K. The star represents the case with $BT_{7.3}$-BT_{11} larger than –10 K.

In the cold season, the inversion strength can be estimated by the linear combination of BT_{11}, $BT_{7.3}$ - $BT_{11,}$ and $(BT_{7.3}$ - $BT_{11})^2$, with the coefficients determined by linear regression, when $BT_{7.3}$ - BT_{11} is larger than –10 K. In this study, the equations used to retrieve inversion strength are:

$$INVST = a_0 + a_1 * BT_{11} + a_2 * (BT_{7.3} - BT_{11}) + a_3 * (BT_{7.3} - BT_{11})^2$$

The coefficients are a_0, a_1, a_2, and a_3. When $BT_{7.3}$-BT_{11} is less than –30 K, the estimated inversion strength is defined as 0 K. In the cold season, there are a few cases with $BT_{7.3}$-BT_{11} between –30 K and –10 K, and inversion strength are 0 K for some cases and larger than 0 K for the others. The estimated inversion strength is defined to linearly increase from 0 K to 2 K when $BT_{7.3}$-BT_{11} increase from –30

K to –10 K. In this study, one set of regression coefficients in the inversion strength retrieval equation is determined for each year from 1980 through 1996, based on all the matched pairs between TOVS brightness temperature and inversion strength from radiosonde data in that year.

After getting the retrieval equation coefficients for each year, the initial TOVS clear-sky BTs are converted to inversion strength using the inversion strength retrieval equations. Then the estimated inversion strength is mapped to the 100 km x 100 km Equal-Area Scalable Earth Grid (EASE-Grid) based on longitude and latitude of the original TOVS data. For each day, a composite map of clear-sky inversion strength over the region north of 60°N is created. The monthly mean inversion strength on each EASE-Grid is calculated as the mean of all the daily composite inversion strength on that grid in a month, which include inversion strength equal zero. The seasonal mean inversion strength is derived as the mean of monthly mean in that season. Only BTs from two channels are used to derive the inversion strength, so the retrieved strength is called the 2-channel statistical inversion strength.

Result

Figure 2 gives the spatial distribution of monthly mean statistical inversion strength in Arctic under clear-sky condition in November, December, January, February, March, and winter (DJF) averaged over the period 1980-1996. The spatial distributions of statistical inversion strength have similar pattern in Arctic from November to March, but with different magnitudes. The lowest statistical inversion strength is over GIN Seas, Barents Sea, and North Europe, which is attributable to the turbulent mixing over open water and high cloud cover in this region during the winter time (Serreze et al. 1992); The mean statistical inversion strength increases eastward, then followed by the decrease over Alaska Region. Over land, the strong statistical inversion strength is over North Russia and North Canada, with the strongest near several river valleys in North Russia due to the strong radiation cooling under clear conditions. Over Arctic Ocean, the mean statistical inversion strength has the highest value over the pack ice in Canada Basin, then decrease radially outward, with the lowest values in the coastal regions north of North Russia and Alaska region.

Over ocean, the mean statistical inversion strength has the highest value in February and lowest value in November, around 16 K in February and 12 K in November over the pack ice in Canada Basin. Over North Europe, the highest statistical inversion strength is in January and February, and lowest value in November and March. Over North Russia and Alaska Region, the highest statistical inversion strength is in January, and lowest value in March. The North Canada has the highest value in January and lowest value in November.

The monthly trend of the 2-channel statistical inversion strength over Arctic region under clear conditions in November, December, January, February, March, and winter (DJF) from 1980-1996 is shown in Figure 3 based on the monthly mean data, and the trend with confidence level larger than 90% based on F test is labeled with + symbol in the figure. The trend distribution has similar pattern in December, January, and February. As the trend shown as the winter average, which is based on the seasonal mean statistical inversion strength, the inversion strength decreases over Laptev Sea and Chukchi Sea with average rate around –0.15 K/Year; the inversion strength decreases over northern Europe with average rate around –0.13 K/Year; the inversion strength increases over North Central

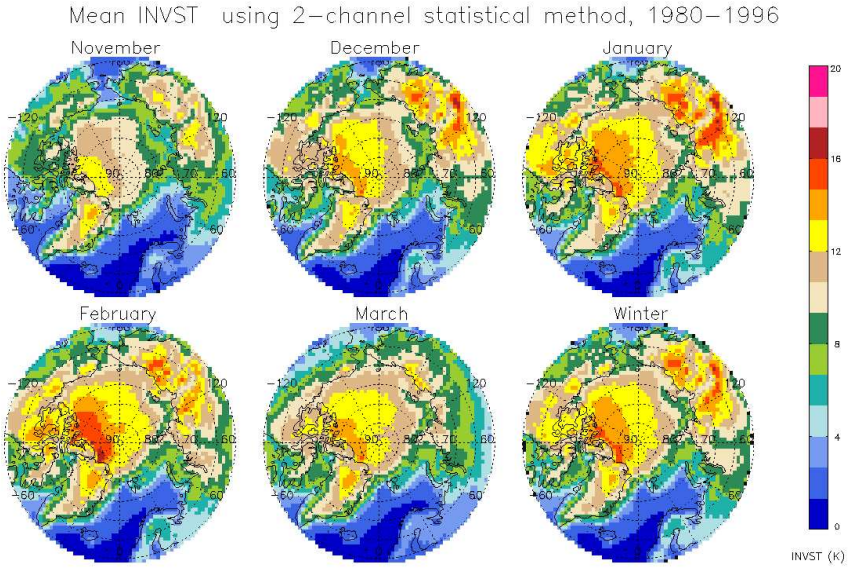

Fig. 2: Monthly mean clear-sky inversion strength (K) in November, December, January, February, March, and winter (DJF) over 1980-1996 using 2-channel statistical method.

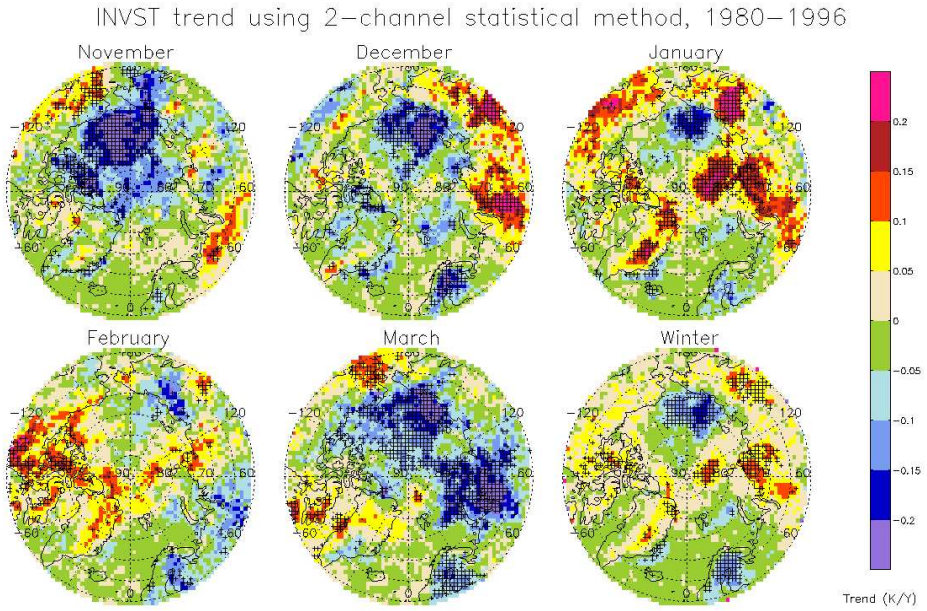

Fig. 3: Monthly trend of clear-sky inversion strength (K/Year) in November, December, January, February, March, and winter (DJF) over 1980-1996 using 2-channel statistical method. The trend with confidence level larger than 90% based on F test is labeled with +.

Russia with rate around 0.1 K/Year; and the increases are also over part of Northeastern Russia, and region between Sevemaya Zemlya and north pole with rate of 0.13 K/Year. All the changes are statistically significant over 90% confidence level based on F-test. Also, the inversion strength increases over some region of North Canada, Canada Archipelago Seas. In March, the inversion strength decreases significantly over Laptev Sea, Chukchi Sea, and Beaufort Sea with the rate over –0.1 K/Year; and decreases in regions surrounding Novaya Zemiya, and over North Central Russia with the rate over –0.1 K/Year; the decreasing rate over North Europe is over –0.05 K/Year. In November, the significant decrease of the inversion strength is over Chukchi Sea, and Beaufort Sea with the rate over –0.1 K/Year; there is insignificant increase of inversion strength over the region between North Europe and North Central Russia with the rate around 0.1 K/Year. In both March and November, there is significant increase over part of Alaska Region with the rate around 0.08 K/Year.

Summary

The 17-year time series of clear-sky temperature inversion strength in the cold season in Arctic is derived from TOVS data using both 2-channel statistical method, and based on TOVS retrieved temperature profiles. Both the 2-chanel statistical and profile monthly mean inversion strength have similar spatial distribution, but the profile inversion strength monthly mean has smaller magnitude. For the 2-channel statistical retrieval method, using one retrieval equation for each year from 1980 through 1996 alleviates the inter-satellite calibration problem. The satellite derived clear-sky monthly mean and trends of 2-channel statistical inversion strength agree well with the weather station based all-sky monthly mean and trends of inversion strength in the cold season, while the profile monthly mean inversion strength has low bias. The weakest temperature inversion in the cold season is over Norwegian Sea, Barents Sea, and over North Europe and increases eastward. Inversion strength has the larger mean value over the pack ice and highest value near several river valleys in the Euroasian Arctic. Over ocean, the monthly mean inversion strength has the highest value in February and lowest value in November. Over land, the highest monthly mean inversion strength is in January, and lowest value in March.

Acknowledgments

This research was supported by NOAA and NSF grants OPP-0240827 and OPP-0230317. The views, opinions, and findings contained in this report are those of the authors and should not be construed as an official National Oceanic and Atmospheric Administration or U.S. Government position, policy, or decision.

References

Andreas, E. L., 1980: Estimation of heat and mass fluxes over Arctic leads. Mon. Wea. Rev., 108, 2057-2063.

Andreas, E. L., and B. Murphy, 1986: Bulk transfer coefficients for heat and momentum over leads and polynyas. J. Phys. Oceanogr., 16, 1875-1883.

Barrie, L. A., J. W. Bottenheim, R. C. Schnell, P. J. Crutzen, and R. A. Rasmussen, 1988: Ozone

destruction and photochemical reactions at polar sunrise in the lower Arctic atmosphere. Nature, 334, 138-141.

Barry, R. G., and M. W. Miles, 1988: Lead patterns in Arctic sea ice from remote sensing data: characteristics, controls and atmospheric interactions. Extended Abstracts Volumn, Second Conference on Polar Meteorology and Oceanography, American Meteorological Society. March 29-31, 1988, Madison, Wisconsin, U.S.A.

Busch, N., U. Ebel, H. Kraus, and E. Schaller, 1982: The structure of the subpolar inversion-cpped ABL. Arch. Met. Geophys. Bioklim., 31A, 1-18.

Chedin, A., N. A. Scott, C. Wahiche, and P. Moulinier, 1985: The improved initialization inversion method: A high resolution physical method for temperature retrievals from satellites of the TIROS-N series. J. Clim. Appl. Meteorol., 24., 128-143.

Curry, J., 1983: ON the formation of polar continental air. J. Atmos. Sci., 40, 2278-2292.

Curry, J. A., W. B. Rossow, D. Randall, and J. L. Schramm. (1996). Overview of Arctic cloud and radiation characteristics. *J. Climate*, 9, 1731-1764.

Francis, J. A. 1994: Improvements to TOVS retrievals over sea ice and applications to estimating Arctic energy fluxes. *J. Geophys. Res.*, 99(D5), 10,395-408.

Kahl, J. D., 1990: Characteristics of the low-level temperature inversion along the Alaskan arctic coast. *Int. J. Climatol*., 10, 537-548.

Liu, Y. and J. Key, 2003: Detection and analysis of clear sky, low-level atmospheric temperature inversions with MODIS, *J. Atmos. Ocean. Tech*., 20, 1727-1737.

Maykut, G. A., and P.E. Church, 1973: Radiation climate of Barrow, Alaska, 1962-66. J. Appl. Meteor., 12, 620-628.

Serreze, M. C., J. D. Kahl and R. C. Schnell, 1992: Low-level temperature inversions of the Eurasian Arctic and comparisons with Soviet drifting stations. *J. Climate*, 5, 615-630.

Vowinkel, E., and S. Orvig, 1970: The climate of the North Polar Basin. World Survey of Climatology, Vol. 14: Climates of the Polar Regions, S. Orvig, Ed., Elsevier, 129-226.